Physics Letters A 378 (2014) 3070–3073

Contents lists available at ScienceDirect

Physics Letters A

www.elsevier.com/locate/pla

Third-order model of thermal conductivity for random polydisperse particulate materials using well-resolved statistical descriptions from tomography

A. Gillman, K. Matouš *

Department of Aerospace and Mechanical Engineering, University of Notre Dame, Notre Dame, IN 46556, USA

ARTICLE INFO

Article history:
Received 23 June 2014
Accepted 16 August 2014
Available online 1 September 2014
Communicated by R. Wu

Keywords:
Heterogeneous materials
Effective material properties
Statistical micromechanics
Adaptive interpolation/integration

ABSTRACT

For heterogeneous materials, obtaining an accurate statistical description has remained an outstanding problem. We accurately evaluate the three-point microstructural parameter that arises in third-order bounds and approximations of effective material properties. We propose new adaptive methods for computing n-point probability functions obtained from three-dimensional microstructures. We show that for highly packed systems our methods result in a 45% accuracy improvement compared to the latest techniques, and third-order approximations agree well with simulation data. Furthermore, third-order estimates of the effective behavior are computed for tomographically characterized systems of highly filled polydisperse ellipsoids and cuboids for the first time.

1. Introduction

The accurate characterization of many-body systems is a long studied problem with applications in many scientific fields at a variety of length scales from molecular arrangements [1,2] up to heterogeneous material microstructures [3] and celestial bodies [4–6]. Often, these systems have varying degrees of randomness at short and long range scales and often only lend themselves to statistical characterization. However, obtaining accurate higher order statistical correlations of many-body systems has proved difficult and is a limiting factor in understanding their physical processes.

Of particular interest in this Letter is determining effective transport and mechanical properties of many particle composites from higher order statistical data, which is a fundamental problem that has captured the attention of great minds including Einstein [7] and Maxwell [8]. The past fifty years have seen the formulation of rigorous bounds and approximations relying on a higher order statistical description of microstructures [9–12]. Especially third-order models have shown good agreement with experimental data [3]. While many theoretical advancements have been made for both linear and nonlinear material behavior [3,13,14], demonstration of these theories has been severely restricted to strong microstructural assumptions due to difficulties in accurately characterizing complex configurations. Various approximations have been formulated to describe complex configurations of random spheres [15–17], but direct computation of the statistical functions in three dimensions with resolution required in third-order models has been elusive.

In this Letter, we present adaptive methods rooted in computational mechanics and high performance computing for efficiently obtaining statistical functions without utilizing approximations of the shape and spatial configuration for random particulate systems. Third-order bounds and approximations of the effective thermal conductivity are computed using this high-fidelity statistical description. These computational methods, which we rigorously verify, allow for computation of statistical descriptors directly from complex three-dimensional microstructures with unprecedented accuracy. We show that previously formulated approximations of these statistical functions for systems of impenetrable monodisperse spheres result in significant inaccuracies, especially at higher volume fractions. Moreover, we extend these methods to other shapes, e.g. crystals, while accounting for degree of polydispersity. For the first time, we compute third-order bounds and approximations of the effective thermal conductivity for tomographically characterized three-dimensional packs of polydisperse ellipsoids and cuboids.

2. Theory of effective material behavior

In this Letter, we explore the effective behavior of steady-state heat conduction described by the conservation of energy assuming Fourier's law. Utilizing the variational principles of minimum

* Corresponding author.
E-mail address: kmatous@nd.edu (K. Matouš).

http://dx.doi.org/10.1016/j.physleta.2014.08.032
0375-9601/

energy and minimum complementary energy assuming ergodicity, statistical and material isotropy, Beran [18] derived third-order bounds of the effective conductivity, κ_e. Torquato [19] and Milton [10] independently simplified these bounds for two-phase composites to $\kappa^L \leq \kappa_e \leq \kappa^U$, where

$$\kappa^L = c_p\kappa_p + c_m\kappa_m - \frac{c_m c_p(\kappa_p-\kappa_m)^2}{c_m\kappa_p + c_p\kappa_m + 2\left(\frac{\zeta_p}{\kappa_p}+\frac{\zeta_m}{\kappa_m}\right)^{-1}}. \tag{1}$$

In this formulation, the bounds depend on the individual phase conductivities κ_i ($i = m$ (matrix) or p (particle)), the volume fractions c_i, and the microstructure parameters ζ_i. This microstructural parameter depends on the one-, two- and three-point probability functions ($S_i = c_i$, S_{ii}, and S_{iii}) and is defined as

$$\zeta_i = \frac{9}{2c_p c_m}\int \frac{3\cos^2\theta - 1}{2r_1 r_2}\tilde{S}_{iii}(r_1, r_2, \theta)\mathrm{d}(\cos\theta)\,\mathrm{d}r_1\,\mathrm{d}r_2, \tag{2}$$

where

$$\tilde{S}_{iii}(r_1, r_2, \theta) = S_{iii}(r_1, r_2, \theta) - \frac{S_{ii}(r_1)S_{ii}(r_2)}{c_i}. \tag{3}$$

For isotropic two-phase systems, Torquato [20] derived a three-point approximation (TPA) that has shown good agreement with simulations [21]. This estimate is given as

$$\frac{\kappa_e}{\kappa_m} = \frac{1 + 2c_p\beta_{pm} - 2c_m\zeta_p\beta_{pm}^2}{1 - c_p\beta_{pm} - 2c_m\zeta_p\beta_{pm}^2}, \tag{4}$$

where

$$\beta_{pm} = \frac{\kappa_p - \kappa_m}{\kappa_p + 2\kappa_m}. \tag{5}$$

While these bounds and approximations were derived decades ago, progress has been slow in accurately determining the microstructural parameter ζ_i (Eq. (2)) due to difficulties in computing the n-point probability function in Eq. (3). For highly filled random particulate composites, no one has been able to compute the probability functions from three-dimensional domains with the fidelity required by these third-order models. As analytical expressions of the n-point probability functions do not generally exist for composites with random configurations, a Monte Carlo-based statistical sampling algorithm is utilized. The accuracy of this method is $\mathcal{O}(1/\sqrt{N_r})$, where N_r is the number of random samples used to compute one function value of $S_{iii}(r_1, r_2, \theta)$, $S_{ii}(r)$, or S_i. A random sample consists of a random translation (described by 3 position values) and random rotation (described by three angles) of a $(n-1)$-simplex within the three-dimensional material domain. To speed up the analysis, we use high performance computing, where the N_r random samples are decomposed on $\mathcal{O}(10^3)$ computing cores. Others [22,23] have attempted a Monte Carlo sampling strategy to compute the probability functions, but on regular structured grids.

3. Adaptive interpolation and sampling method

Since computations on a structured grid are inefficient, we propose an adaptive triangulation technique. This method involves iteratively constructing a Delaunay triangulation of tetrahedrons, which we will refer to as $\mathcal{T}$, to create an interpolant of $\tilde{S}_{iii}(r_1, r_2, \theta)$ with C^0 continuity. Summarizing the algorithm, an initial regular tetrahedral grid is constructed for the domain $[r_1 = 0, r_1 = r^\infty] \times [r_2 = 0, r_2 = r_1] \times [\theta = 0, \theta = \pi]$ (note that this is half of the integration domain since the function is symmetric about the axis $r_1 = r_2$). This triangulation and associated

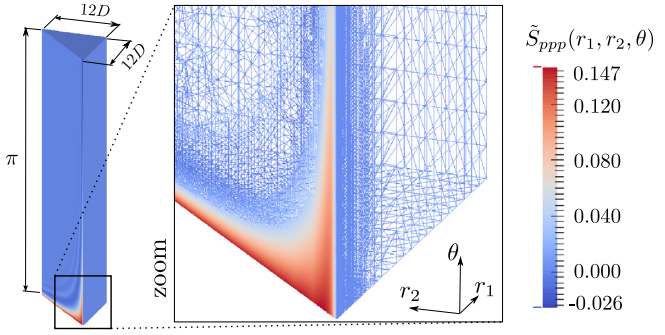

Fig. 1. Illustration of resulting adaptive triangulation of $\tilde{S}_{iii}(r_1, r_2, \theta)$ for system of impenetrable monodisperse spheres with $c_p = 0.6$.

function values, $\tilde{S}_{iii}(r_1, r_2, \theta)$ which appear in the integral kernel of Eq. (2), define the initial interpolant $\mathcal{T}_{l=0}$ (l is the adaptive iteration level). For a given iteration, a bisection method is used to refine the triangulation based on the local error of the statistics. For all tetrahedrons in a given iteration of the interpolant $\mathcal{T}_l$, the local accuracy is evaluated at each edge midpoint by considering the difference between the interpolated and computed probability functions. If an edge midpoint does not satisfy the error indicator function $\epsilon_a = \left|\tilde{S}_{iii}(r_1, r_2, \theta) - \mathcal{T}_l(r_1, r_2, \theta)\right| < tol$, where tol is a set tolerance, each edge of the tetrahedron is bisected and added to $\mathcal{T}_{l+1}$. If all midpoints in a tetrahedron satisfy ϵ_a, the tetrahedron is added to $\mathcal{T}_{l+1}$ unchanged. This iterative process is repeated until all grid points satisfy the error indicator function. After a convergence study, it was determined that $tol = (1/200)\max\{\tilde{S}_{iii}(r_1, r_2, \theta)\}$ results in low numerical error for all computations presented in this Letter. An example of the resulting triangulation for a highly filled ($c_p = 0.6$) monodisperse system of spheres with diameter D is shown in Fig. 1. Note that this function is 0 in a majority of the domain, but sharp variations exist near the origin ($r_1 = 0, r_2 = 0, \theta = 0$), along the diagonal $r_1 = r_2$ and near the edge of the domain where $r_1 = r_2 = 0$. The triangulation for this example contains $\mathcal{O}(10^7)$ tetrahedrons with a minimum edge length of $2.78 \cdot 10^{-17}D$, a mean edge length of $3.61 \cdot 10^{-2}D$, and a maximum edge length of $1.55D$, thus revealing the wide range of length scales required for accurately representing this function. The resulting interpolant $\mathcal{T}$ is then used as the basis for computing ζ_i via simplex integration of Eq. (2). In this work, Monte Carlo integration of each tetrahedron is performed. A convergence study determined that using $N_{int} = 1000$ random integration points per tetrahedron is sufficient for all microstructures presented in this Letter. Given that there are $\mathcal{O}(10^7)$ tetrahedrons in a typical interpolant, $\mathcal{O}(10^{10})$ integration points are required to evaluate the integral (2).

4. Verification

The proposed adaptive triangulation technique is verified by considering a two-phase system of overlapping spheres, which is one of a few configurations where the n-point probability functions of the matrix phase m can be defined analytically as:

$$S_{m\ldots m}(\boldsymbol{x}_1, \boldsymbol{x}_2, \ldots, \boldsymbol{x}_n) = \exp(-\rho V_n) \tag{6}$$

Here, ρ is the number density of spheres and V_n is the union volume of n spheres with diameter D. Considering four volume fractions of this model, ζ_m was computed with $r^\infty = 6D$. The results and errors associated with the computations are provided in Table 1. An error measure is defined as $\varepsilon_{PS} = \left|\zeta_m - \zeta_m^{R1}\right|/\zeta_m^{R1} \times 100$ [%], where ζ_m is the result from this work, and ζ_m^{R1} is the most accurate result presented in the literature [24]. Note that all

Table 1
Verification of the adaptive interpolation and integration method for computing Eq. (2) assuming penetrable sphere model. Comparison is made between results of this work (ζ_m) and results in [24] (ζ_m^{R1}).

c_p	ζ_m	ζ_m^{R1}	ε_{PS}
0.2	0.5187	0.5174	0.24%
0.4	0.6571	0.6489	1.26%
0.6	0.7743	0.7702	0.54%
0.8	0.9039	0.8866	1.95%

Table 2
Comparison of ζ_p for random impenetrable monodisperse sphere systems. Comparison is made between results presented in this work (ζ_p) and results in [17] (ζ_p^{R2}).

c_p	ζ_p	ζ_p^{R2}	ε_{IS}
0.2	0.0442	0.0409	8.17%
0.4	0.0883	0.0765	15.37%
0.5	0.1114	0.0938	18.78%
0.6	0.1967	0.134	46.78%

results for ζ_m are within 2%. This verifies our adaptive triangulation technique.

Following verification of the adaptive interpolation and integration method, packs of impenetrable monodisperse spheres were considered. Such systems have been studied extensively by Torquato and collaborators [15–17]. However, despite significant progress, computing the microstructural parameter for three-dimensional systems directly has been unachievable until this Letter due to the complexity of the n-point probability functions. The hard sphere systems were generated using a packing algorithm [25] based on the Lubachevsky–Stillinger method [26,27]. Cubic domains consisting of $\mathcal{O}(10^4)$ particles with diameter D were generated using a high expansion rate to ensure statistical isotropy. After a convergence study, it was determined that $r^{\infty} = 12D$ is required to compute ζ_p with acceptable accuracy. Furthermore, the convergence study revealed that it is necessary to use $N_r = 10^7$ random samples for each n-point probability function evaluation in Eq. (3) to satisfy the tight tolerance *tol*. The results are presented in Table 2 and are compared with the best known approximations given in [17], denoted here as ζ_p^{R2}. The improvement of ζ_p from ζ_p^{R2} is quantified by introducing an error metric $\varepsilon_{IS} = |\zeta_p - \zeta_p^{R2}|/\zeta_p^{R2} \times 100$ [%]. Note that reasonable agreement is shown for lower volume fractions, but significant improvement has been achieved for higher volume fractions. ζ_p is then used to compute the lower bound (Eq. (1)) and TPA (Eq. (4)) of κ_e for a contrast ratio of $\kappa_p/\kappa_m = \infty$, and the results are presented in Fig. 2. These calculations are also compared to simulation data (circles) given in [21]. Excellent agreement is shown between the TPA with well resolved (WR) statistics, which we denote WR-TPA, and the simulation data. Note that all differences are below 2%, thus verifying the Monte Carlo statistical sampling technique within our adaptive triangulation framework. Note that the WR-three-point lower bound (dashed line) has been improved from [17] (dotted line) by 4.53%, and the WR-TPA (solid line) has been improved from [17] (dash-dotted line) by 17.8% for the $c_p = 0.6$ volume fraction case.

5. Examples

Following the rigorous verification of well-studied systems, third-order bounds and approximations for materials with arbitrary particle shapes and dispersity are analyzed. This demonstrates that a large class of systems, which have been previously unfeasible to study, can now be examined. Note that realizations of these systems can be generated from imaging methods [28] or from packing algorithms [29], but the characterization techniques are not the focus of this Letter. These characterization

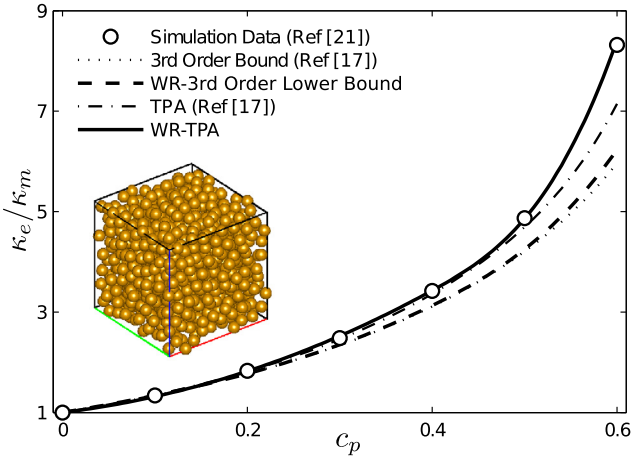

Fig. 2. Third-order lower bound and approximation of κ_e for random systems of impenetrable monodisperse spheres for $\kappa_p/\kappa_m = \infty$. The dotted and dash-dotted lines correspond to computations using ζ_p^{R2} from Ref. [17], while the solid and dashed lines employ ζ_p with well resolved (WR) statistics. The circles represent simulation data from [21]. The inset image is a representative subsection of the pack with $c_p = 0.6$.

techniques have been demonstrated in [28], for example. In this Letter, highly filled polydisperse systems are characterized using X-ray computer tomography, which has become a viable method for non-destructively obtaining accurate three-dimensional representations [30,23]. Samples are prepared with a manual randomized packing strategy while limiting sample boundary effects. The three samples studied in this Letter contain (i) polydisperse spherical particles (mustard seed), (ii) polydisperse ellipsoidal particles (Teff grains), and (iii) polydisperse cuboids (salt crystals). Consistent with the packs of monodisperse spheres analyzed above, $\mathcal{O}(10^4)$ particles are contained in each sample. These samples are tomographically characterized and image processing algorithms are used to identify individual particles. Then, all particles in the resulting voxelized data set are modeled as idealized shapes in order to provide a description of the micro-computed tomography data in continuous Euclidean space, reduce the data set size, and thus improve the understanding of these complex systems. See our prior work for details of these characterization steps [28].

The distributions of particles with an inset image of a representative sub-volume of the system for each tomographically characterized pack are shown in Fig. 3. In these figures, the variable d and s are the representative sphere diameter (diameter computed from volume of a particle assuming a spherical shape) and representative cube side length (side length of a cube computed from volume of particle assuming a cubic shape), respectively. The parameter, e, measures the eccentricity of a particle (ratio of semi-axes a, b, and c) and is computed as $e = \frac{1}{3}\left(\frac{\sqrt{a^2-b^2}}{a} + \frac{\sqrt{b^2-c^2}}{b} + \frac{\sqrt{a^2-c^2}}{a}\right)$, where $a > b > c$. $e = 0$ corresponds to a sphere and a cube, respectively. Considering the distributions in Fig. 3, the system of nearly spherical grains (Fig. 3(a)) contains particles with low eccentricity and an average representative diameter of $\bar{d} = 1.87$ mm. The average semi-axis lengths are $\bar{a} = 1.044$ mm, $\bar{b} = 0.940$ mm, and $\bar{c} = 0.843$ mm. The system of more eccentric ellipsoids (Fig. 3(b)) has mean geometric properties of $\bar{d} = 0.686$ mm, $\bar{a} = 0.535$ mm, $\bar{b} = 0.285$ mm, and $\bar{c} = 0.266$ mm. The system of cuboidal particles (Fig. 3(c)) has mean geometric properties of $\bar{s} = 0.296$ mm, $\bar{a} = 0.161$ mm, $\bar{b} = 0.142$ mm, and $\bar{c} = 0.142$ mm, which indicate nearly cubic particles with low eccentricities.

Using the idealized shape representation of these systems within the adaptive triangulation and Monte-Carlo based statistical sampling methods, the microstructural parameter ζ_p is computed

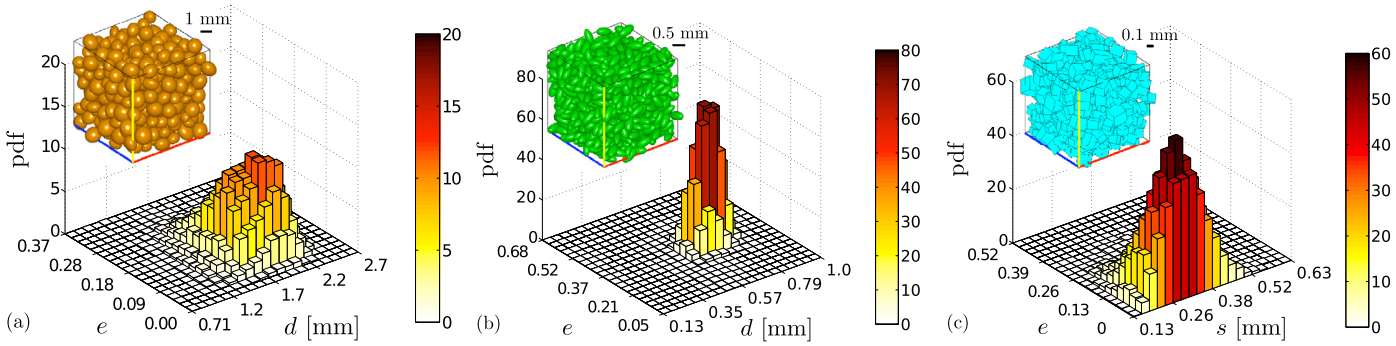

Fig. 3. Distributions of particles for tomographically characterized systems. (a) Distribution for pack of spheres. (b) Distribution for pack of ellipsoids. (c) Distribution for pack of cuboids. In these figures, d, s, and e are the representative sphere diameter, representative cube diameter, and eccentricity. The inset figure of each distribution shows a representative subsection of each system.

Table 3
Three-point lower bound $\kappa_e^{\text{WR-L}}$ and approximation $\kappa_e^{\text{WR-TPA}}$ with well resolved (WR) statistics for polydisperse systems of spheres, ellipsoids, and cuboids assuming $\kappa_p/\kappa_m = \infty$.

Pack type	c_p	ζ_p	$\kappa_e^{\text{WR-L}}/\kappa_m$	$\kappa_e^{\text{WR-TPA}}/\kappa_m$
Spheres	0.682	0.2441	8.826	13.38
Ellipsoids	0.619	0.2378	6.891	10.30
Cuboids	0.568	0.3266	6.226	12.39

using the same parameters given for the monodisperse impenetrable spheres ($N_r = 10^7$ and $r^\infty = 12$ $\{\bar{d}$ or $\bar{s}\}$). The resulting values and associated well-resolved lower bounds (WR-L) and WR-TPAs of κ_e are given in Table 3. The shape effect and degree of dispersity of these systems result in higher values of ζ_p, when compared to the monodisperse sphere systems. This leads to higher effective conductivities for a given volume fraction.

6. Conclusions

In conclusion, we have demonstrated that effective properties of highly filled random polydisperse particulate systems can be computed with unprecedented accuracy from rich three-dimensional microstructural data. We have described novel adaptive methods for computing third-order bounds and approximations of the effective thermal conductivity for polydisperse composites. With these techniques, proper assessment of the rich mathematical history in computing effective material properties including diffusivity, magnetic and fluid permeability, etc. is now realizable. Furthermore, extension to a wide array of particle types including any Platonic or Archimedean solid is now possible. As random and heterogeneous many-body systems are common in several fields, use of these statistical characterization techniques has wide ranging application in physics, e.g. molecular arrangements, celestial configurations, and beyond.

References

[1] D. Srolovitz, T. Egami, V. Vitek, Phys. Rev. B 24 (1981) 6936.
[2] F. Wooten, K. Winer, D. Weaire, Phys. Rev. Lett. 54 (1985) 1392–1395.
[3] S. Torquato, Random Heterogeneous Materials: Microstructure and Macroscopic Properties, vol. 16, Springer, 2002.
[4] H. Totsuji, T. Kihara, Publ. Astron. Soc. Jpn. 21 (1969) 221.
[5] H.K. Eriksen, F.K. Hansen, A.J. Banday, K.M. Górski, P. Lilje, Astrophys. J. 605 (2004) 14.
[6] Y. Wiaux, P. Vielva, E. Martinez-Gonzalez, P. Vandergheynst, Phys. Rev. Lett. 96 (2006) 151303.
[7] A. Einstein, Ann. Phys. (Leipz.) 324 (1906) 289–306.
[8] J. Maxwell, A Treatise on Electricity and Magnetism, vol. 1, Clarendon Press, 1873.
[9] Z. Hashin, S. Shtrikman, J. Appl. Phys. 33 (1962) 3125–3131.
[10] G.W. Milton, Phys. Rev. Lett. 46 (1981) 542.
[11] S. Torquato, Phys. Rev. Lett. 79 (1997) 681.
[12] J.R. Willis, in: H.G. Hopkins, M.J. Sewell (Eds.), Mechanics of Solids: The Rodney Hill 60th Anniversary Volume, Pergamon Press, 1982, pp. 653–686.
[13] G.W. Milton, The Theory of Composites, vol. 6, Cambridge University Press, 2002.
[14] P.P. Castañeda, Phys. Rev. B 57 (1998) 12077.
[15] J. Beasley, S. Torquato, J. Appl. Phys. 60 (1986) 3576–3581.
[16] S. Torquato, F. Lado, Phys. Rev. B 33 (1986) 6428.
[17] C. Miller, S. Torquato, J. Appl. Phys. 68 (1990) 5486–5493.
[18] M. Beran, Nuovo Cimento 10 (38) (1965) 771–782.
[19] S. Torquato, Microscopic approach to transport in two-phase random media, Ph.D. Thesis, 1980.
[20] S. Torquato, J. Appl. Phys. 58 (1985) 3790–3797.
[21] I.C. Kim, S. Torquato, J. Appl. Phys. 69 (1991) 2280–2289.
[22] D.A. Coker, S. Torquato, J. Appl. Phys. 77 (1995) 6087–6099.
[23] H. Lee, M. Brandyberry, A. Tudor, K. Matouš, Phys. Rev. E 80 (2009), 061301-1–061301-12.
[24] A. Helte, Proc. R. Soc. Lond. Ser. A, Math. Phys. Sci. 450 (1995) 651–665.
[25] M. Skoge, A. Donev, F. Stillinger, S. Torquato, Phys. Rev. E 74 (2006) 041127.
[26] B. Lubachevsky, F. Stillinger, J. Stat. Phys. 60 (1990) 561–583.
[27] A. Donev, S. Torquato, F. Stillinger, J. Comput. Phys. 202 (2005) 737–764.
[28] A. Gillman, K. Matouš, S. Atkinson, Phys. Rev. E 87 (2013) 022208.
[29] D.S. Stafford, T.L. Jackson, J. Comput. Phys. 229 (2010) 3295–3315.
[30] T. Aste, M. Saadatfar, T. Senden, Phys. Rev. E 71 (2005) 061302.